EINDHOVEN UNIVERSITY OF TECHNOLOGY

Nucleation and growth of Pt atomic layer deposition on Al2O3 substrates using (methylcyclopentadienyl)-trimethyl platinum and O2 plasma

Citation for published version (APA):
Baker, L., Cavanagh, A. S., Seghete, D., George, S. M., Mackus, A. J. M., Kessels, W. M. M., Liu, Z. Y., & Wagner, F. T. (2011). Nucleation and growth of Pt atomic layer deposition on Al2O3 substrates using (methylcyclopentadienyl)-trimethyl platinum and O2 plasma. *Journal of Applied Physics*, *109*(8), 084333-1/10. Article 084333. https://doi.org/10.1063/1.3555091

DOI:
10.1063/1.3555091

Document status and date:
Published: 01/01/2011

Document Version:
Publisher's PDF, also known as Version of Record (includes final page, issue and volume numbers)

Please check the document version of this publication:

• A submitted manuscript is the version of the article upon submission and before peer-review. There can be important differences between the submitted version and the official published version of record. People interested in the research are advised to contact the author for the final version of the publication, or visit the DOI to the publisher's website.
• The final author version and the galley proof are versions of the publication after peer review.
• The final published version features the final layout of the paper including the volume, issue and page numbers.

Link to publication

General rights
Copyright and moral rights for the publications made accessible in the public portal are retained by the authors and/or other copyright owners and it is a condition of accessing publications that users recognise and abide by the legal requirements associated with these rights.

• Users may download and print one copy of any publication from the public portal for the purpose of private study or research.
• You may not further distribute the material or use it for any profit-making activity or commercial gain
• You may freely distribute the URL identifying the publication in the public portal.

If the publication is distributed under the terms of Article 25fa of the Dutch Copyright Act, indicated by the "Taverne" license above, please follow below link for the End User Agreement:

www.tue.nl/taverne

Take down policy
If you believe that this document breaches copyright please contact us at:

openaccess@tue.nl

providing details and we will investigate your claim.

Download date: 07. Jul. 2024

Nucleation and growth of Pt atomic layer deposition on Al_2O_3 substrates using (methylcyclopentadienyl)-trimethyl platinum and O_2 plasma

L. Baker,[1] A. S. Cavanagh,[1] D. Seghete,[1] S. M. George,[1,a)] A. J. M. Mackus,[2] W. M. M. Kessels,[2] Z. Y. Liu,[3] and F. T. Wagner[3]
[1]*Department of Chemistry and Biochemistry and Department of Chemical and Biological Engineering, University of Colorado, Boulder, Colorado 80309, USA*
[2]*Department of Applied Physics, Eindhoven University of Technology, P.O. Box 513, 5600 MB Eindhoven, The Netherlands*
[3]*General Motors Research and Development, Honeoye Falls, New York 14472, USA*

(Received 27 October 2010; accepted 16 January 2011; published online 22 April 2011)

The nucleation and growth of Pt atomic layer deposition (ALD) on Al_2O_3 substrates was studied using (methylcyclopentadienyl)-trimethyl platinum ($MeCpPtMe_3$) and O_2 plasma as the reactants. The nucleation of Pt ALD was examined on Al_2O_3 ALD substrates at 300 °C using a variety of techniques including spectroscopic ellipsometry, x-ray reflectivity, x-ray photoelectron spectroscopy, and scanning electron microscopy. These techniques revealed that Pt ALD does not nucleate and grow immediately on the Al_2O_3 ALD substrates. There was negligible Pt ALD during the first 38 ALD cycles. The Pt ALD growth rate then increased substantially during the next 12 ALD cycles. Subsequently, the Pt ALD growth rate reached a steady state linear growth regime for >50 ALD cycles. These measurements suggest that the Pt ALD first forms a number of nanoclusters that grow slowly during the first 38 ALD cycles. These islands then merge during the next 12 cycles and yield a steady state Pt ALD growth rate of ~0.05 nm/cycle for >50 ALD cycles. The Pt ALD film at the onset of the steady state linear growth regime was approximately 2–3 nm in thickness. However, the SEM images of these Pt ALD films appeared corrugated and wormlike. These films also had a density that was only 50–70% of bulk Pt. Film densities that were consistent with bulk Pt were not observed until after >100 ALD cycles when the Pt ALD films appeared much smoother and were 4–5 nm in thickness. The Pt ALD nucleation rate could be enhanced somewhat using different O_2 plasma parameters. © *2011 American Institute of Physics*. [doi:10.1063/1.3555091]

I. INTRODUCTION

Atomic layer deposition (ALD) is a thin film growth technique utilizing sequential self-limiting surface reactions to deposit films with atomic layer control that are usually extremely conformal to the initial substrate.[1,2] However, there are some prominent exceptions. The nucleation of metal ALD on oxide substrates is very challenging because metals do not easily wet oxide substrates.[3] Consequently, metal ALD on oxide substrates generally results in a dispersion of metal nanoclusters that will form a continuous film only when the metal islands have grown together after numerous ALD cycles. The nonconformality of metal ALD on oxide substrates is linked to the higher surface energy of the metal film relative to the oxide substrate.[3] Given a sufficient metal atom mobility, the metal atoms will diffuse to form metal nanoclusters to minimize the system energy.

In addition to the difficulty of the wetting of the metal ALD film on oxide substrates, achieving nucleation of the metal ALD film on oxide substrates is also extremely difficult. As a result, many ALD cycles are typically required to observe any metal deposition on oxide substrates. This difficulty is related to the absence of the proper surface species to react with the precursors used for metal ALD. The metal precursors may also contain ligands that bind to the oxide substrate and block adsorption sites.[4,5] Consequently, there have been very few reports of the ALD of continuous and conformal ultrathin metal films on oxide substrates. One of the most favorable systems is W ALD on Al_2O_3 substrates where a continuous and conformal W ALD film is obtained after 8–10 ALD cycles.[6–8]

Despite the difficulties, there are many motivations to deposit continuous and conformal ultrathin metal films using ALD. For example, various precious metals used in catalysis need to be employed as efficiently as possible to reduce costs. An ultrathin metal film on a high surface area support would be a very cost effective catalytic substrate. In addition, continuous metal films are important in applications in corrosive environments where the underlying support material would be chemically damaged unless the metal covers the entire support. Continuous ultrathin metal films are also important for fabricating thin film architectures in magnetics and coatings for nanoelectromechanical systems.

Platinum is a precious metal that has many uses in catalysis and electrochemistry. For example, platinum is one of the best catalytic surfaces for the oxidation and reduction reactions in fuel cells.[9,10] Recent research has suggested that ultrathin conformal Pt films on a high surface area support will exhibit significantly higher area-specific activity for the oxygen reduction reaction than an equivalent surface area of Pt nanoparticles.[9,11] The ALD of Pt films can be achieved using

[a)]Author to whom correspondence should be addressed. Electronic mail: steven.george@colorado.edu.

 © 2011 American Institute of Physics

Downloaded 27 Apr 2011 to 131.155.110.244. Redistribution subject to AIP license or copyright; see http://jap.aip.org/about/rights_and_permissions

(methylcyclopentadienyl)-trimethylplatinum ($MeCpPtMe_3$) and O_2.[12] Since the original report of this Pt ALD process, many studies have utilized this surface chemistry for a variety of applications.[13–21] However, this Pt ALD chemistry does not yield continuous and conformal films as is typical for ALD film growth. Pt ALD growth on oxide substrates is characterized by the deposition of dispersed nanoclusters and requires numerous ALD cycles for the initial nucleation and growth of the Pt film.

Recently, plasma Pt ALD using $MeCpPtMe_3$ and O_2 plasma has been reported to yield Pt films that nucleate and grow much more rapidly on SiO_2 than Pt ALD films grown using thermal chemistry.[22,23] The *in situ* spectroscopic ellipsometry (SE) studies that were employed in this earlier work suggest that the Pt ALD process using $MeCpPtMe_3$ and O_2 plasma nucleated and grew from nearly the first ALD cycle. In this paper, the nucleation and growth of Pt ALD on Al_2O_3 ALD surfaces using $MeCpPtMe_3$ and O_2 plasma as reactants is explored utilizing a combination of SE, x-ray reflectivity (XRR), x-ray photoemission spectroscopy (XPS), and scanning electron microscopy (SEM). These combined techniques clarify the details of Pt ALD nucleation and quantify the thickness at which the Pt ALD film is truly continuous on the underlying Al_2O_3 substrates.

II. EXPERIMENTAL

A series of Pt ALD films were grown on Al_2O_3 ALD substrates at Eindhoven University using 1, 5, 10, 25, 38, 50, 68, 75, 88, 100, 125, 150, 200, and 300 ALD cycles. The Pt films were deposited at 300 °C using alternating doses of $MeCpPtMe_3$ and O_2 plasma.[22,23] The Al_2O_3 ALD substrates were grown using trimethylaluminum and O_2 plasma.[24] The thickness of the Al_2O_3 ALD films grown on Si wafers was $\sim$50 nm. The Pt ALD films were deposited in a reactor equipped with an inductively-coupled plasma (ICP) source that has been described previously in detail.[25]

The reactor was pumped by a turbomolecular pump that was backed by a rotary vane mechanical pump. This pumping system was capable of evacuating the reactor to a base pressure of $<1 \times 10^{-5}$ Torr. During the $MeCpPtMe_3$ doses, the gate valve to the pump was closed to maximize usage of the Pt precursor. The $MeCpPtMe_3$ (98% purity from Sigma Aldrich) was held at 70 °C in a sealed vessel and vapor drawn into the reactor. After the Pt precursor exposure, the gate valve was opened to evacuate the reactor. O_2 gas was then flowed through the deposition chamber at 7 mTorr while the 100 W plasma power was applied for 0.5 s.

Another series of Pt ALD films were grown on Al_2O_3 ALD substrates at the University of Colorado. The reactor consisted of a small chamber connected to an ICP plasma source (Litmus Blue, Advanced Energy). The small chamber had several ports for precursor dosing and one port for pumping via a rotary vane mechanical pump. In these growth experiments, Pt ALD films were deposited at 200 °C using the $MeCpPtMe_3$ and O_2 plasma. The O_2 plasma exposures were performed using an oxygen pressure of 0.3 Torr, an ICP RF power of 600 W, and a 5 s plasma exposure time.

Ex situ variable-angle SE measurements were recorded at Eindhoven University on a J.A. Woollam, Inc. M2000D ellipsometer at photon energies between 0.75–6.5 eV as described earlier.[22,26,27] The Pt film was modeled using a Drude-Lorentz parameterization in which the Drude term accounts for the intraband absorption at low photon energies by conduction electrons. XRR measurements were recorded at the University of Colorado on a Bede D1 diffractometer from Bede Scientific Ltd. using Max-flux optics (Osmic, Inc). The x-ray wavelength from the Cu $K\alpha$ x-ray tube was 1.54 Å. XRR was performed with 0.5 mm source and detector slits and a channel-cut-crystal inserted in the incident beam. The Bede REFS software was used to fit the XRR data and determine the density and thickness of the Pt films.

A PHI 5600 x-ray photoelectron spectrometer was used to obtain the XPS spectra of the Pt film samples at the University of Colorado. Monochromatic Al $K\alpha$ X-rays at 1486.6 eV were used for the XPS analysis. The pass energy was 58.7–93.9 eV and the step size was 0.250–0.400 eV. An electron beam neutralizer was employed at 17.8 mA. Data was collected with Auger Scan (RBD Enterprises, Inc., Bend, OR). XPS data was analyzed in CASA XPS (Casa Software Ltd, UK). The XPS spectra were calibrated by setting the adventitious carbon peak to a binding energy of 285 eV. Peak fits for the Pt 4d and Al 2s peaks were obtained using a linear background and 70:30 Gaussian:Lorentzian peaks.

SEM was performed on a Zeiss Ultra 55 microscope at General Motors. This microscope was equipped with a field-emission gun and could operate at various accelerating voltages. All SEM images were recorded using an accelerating voltage of 1 kV and an in-lens secondary electron imaging mode. The contrast was low and images needed to be recorded quickly before the contrast was lost. This loss may have been caused by electron beam-induced deposition of adventitious carbon. Tests with blank samples confirmed that the images were real and not artifacts of instrumental noise.

III. RESULTS AND DISCUSSION

A. Spectroscopic Ellipsometry

Figure 1 shows the Pt ALD film thickness versus the number of ALD cycles from 50 to 200 cycles as determined by *ex situ* SE at Eindhoven University. The thicknesses for each sample are also listed in Table I. The SE measurements reveal that the Pt ALD growth rate is approximately linear after 50 cycles. The measured growth rate of $\sim$0.05 nm/cycle is consistent with the previously reported growth rate of 0.047 nm/cycle for the $MeCpPtMe_3$ and O_2 plasma process.[22] This growth rate is also consistent with the growth rate of $\sim$0.05 nm/cycle reported for thermal Pt ALD using $MeCpPtMe_3$ and O_2 gas.[12]

A linear fit of the Pt ALD film thicknesses versus the number of ALD cycles appears to pass through the origin. This observation suggests that the $MeCpPtMe_3$ and O_2 plasma Pt ALD process has very little or no nucleation delay on Al_2O_3 ALD substrates. However, an earlier *in situ* SE study observed a short nucleation period through the first 50 cycles followed by linear growth.[22] Due to uncertainty in the modeling of ellipsometry spectra of metal nanoclusters on dielectric surfaces, SE exhibits some difficulty in making reliable determinations of the thickness and morphology of

Downloaded 27 Apr 2011 to 131.155.110.244. Redistribution subject to AIP license or copyright; see http://jap.aip.org/about/rights_and_permissions

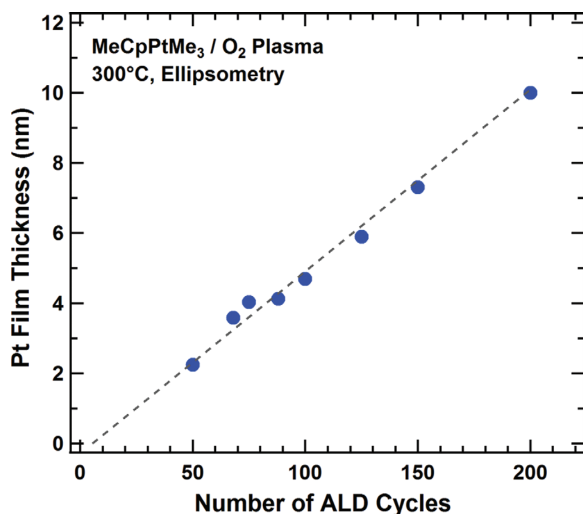

FIG. 1. (Color online) Pt film thickness determined using SE vs number of ALD cycles for Pt ALD films grown on Al_2O_3 using $MeCpPtMe_3$ and O_2 plasma at 300 °C.

metal films during the first few nanometers of film growth.[27] Therefore, the Pt ALD thicknesses for the films grown using 1, 5, 10, 25, and 38 Pt ALD cycles are uncertain and are not shown in Fig. 1.

B. X-ray Reflectivity

Each of the Pt ALD films measured by *ex situ* SE was also analyzed using *ex situ* XRR analysis. In principle, XRR can be used to determine the thickness and density of Pt ALD films ranging in thickness from 0.2 to over 50 nm. The XRR modeling assumes that the films are continuous and the material interfaces present in the sample can be represented by an interfacial region with finite roughness in which the electron density is a composite of the interfacing layers in the film.[28] XRR scans for Pt ALD films grown using 38, 50, 100, and 200 cycles are shown in Fig. 2. An XRR scan is also displayed for the initial Al_2O_3 ALD substrate. The initial Al_2O_3 ALD substrate had a thickness of 51–52 nm with surface roughness < 1 nm RMS. The periodic oscillations with a period of $\sim$300 arc sec result from x-ray interference in the Al_2O_3 ALD film. The Pt ALD film thicknesses that were determined by modeling all of the XRR scans are listed in Table I.

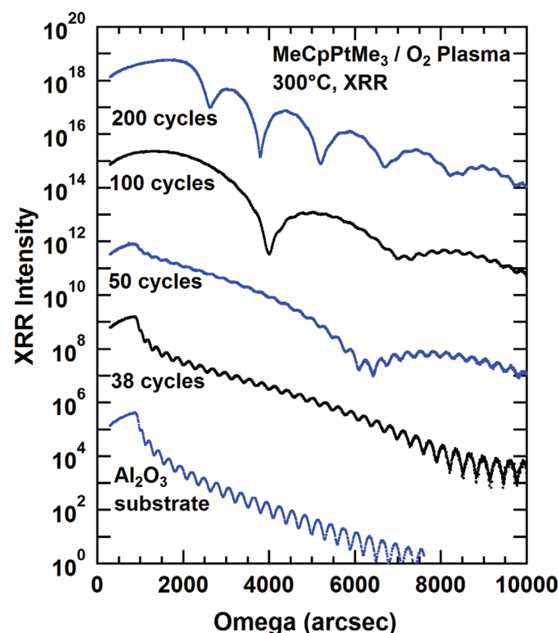

FIG. 2. (Color online) XRR scans for Pt ALD films grown using 0, 38, 50, 100, and 200 ALD cycles on Al_2O_3 using $MeCpPtMe_3$ and O_2 plasma at 300 °C. The summary of all the XRR scans for the various Pt ALD films grown using different numbers of ALD cycles is given in Table I.

As the Pt ALD film thickness increases, a modulation appears in the XRR scans that increases in frequency for the thicker Pt ALD films. For example, the x-ray interference minima at approximately 6500 arc sec in the XRR scan for the Pt ALD film growth using 50 cycles indicate a film thickness of 2.61 nm. The XRR scans also reveal the densities of the Pt ALD films that are included in Table I. The densities are generally lower in the initial nucleation region. The Pt ALD film density reaches >95% of the Pt bulk density for >100 cycles. Table I also shows the adjusted XRR thickness obtained by multiplying the measured XRR thickness by the fraction of the bulk Pt density as determined by the XRR analysis.

Figure 3 shows the Pt ALD thickness determined by XRR measurements versus the number of ALD cycles. The thickness is negligible for 5, 10, 25, and 38 ALD cycles. Figure 2 reveals no interference fringes for the Pt ALD film

TABLE I. Summary of the SE thickness, XRR thickness, XRR density % of bulk Pt, density-adjusted XRR thickness and XPS thickness for films grown on Al_2O_3 vs number of ALD cycles using $MeCpPtMe_3$ and O_2 plasma at 300 °C.

Cycles	SE thickness (nm)	XRR thickness (nm)	XRR Density %	Adjusted XRR Thickness (nm)	XPS Thickness (nm)
25	…	0.01	93	0.01	0.04
38	…	0.17	85	0.14	0.29
50	2.25	2.61	55	1.44	0.97
68	3.59	3.38	70	2.37	1.93
75	4.04	3.77	74	2.79	2.07
88	4.13	4.16	81	3.37	2.61
100	4.7	4.58	93	4.26	3.39
125	5.89	5.78	97	5.61	…
150	7.31	6.91	98	6.77	…
200	10	9.95	96	9.55	…
300	15.5	14.6	97	14.16	

Downloaded 27 Apr 2011 to 131.155.110.244. Redistribution subject to AIP license or copyright; see http://jap.aip.org/about/rights_and_permissions

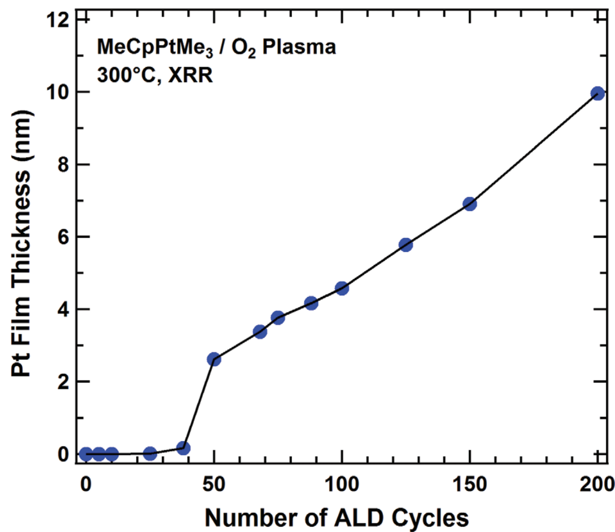

FIG. 3. (Color online) Pt film thickness determined using XRR scans vs number of ALD cycles for Pt ALD films grown on Al_2O_3 using $MeCpPtMe_3$ and O_2 plasma at 300 °C.

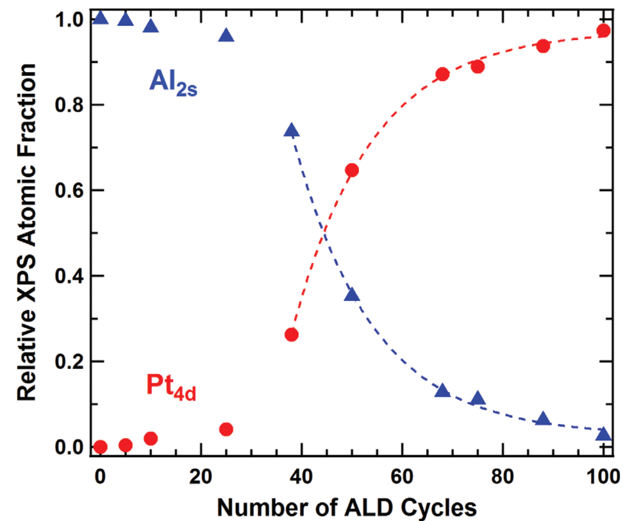

FIG. 4. (Color online) Relative XPS atomic fraction of Al and Pt vs number of ALD cycles for Pt ALD films grown on Al_2O_3 using $MeCpPtMe_3$ and O_2 plasma at 300 °C. The dashed lines show the fit assuming layer-by-layer growth of Pt on the Al_2O_3 substrate.

after 38 cycles. However, there are differences between the XRR scans for the initial Al_2O_3 substrate and for the substrate after 38 cycles. These differences suggest the presence of a perturbing high density material after 38 cycles. The film thickness determined by XRR increases abruptly after 38 ALD cycles and then increases linearly after 50 ALD cycles. A similar progression of the Pt ALD film thickness through 50 ALD cycles was also observed by the earlier SE measurements.[22] However, the transition was not as abrupt for the SE measurements.

C. X-ray Photoemission Spectroscopy

The Pt ALD film samples were analyzed using XPS to assess the surface composition and to determine the film thickness using the Thickogram model.[29] The photoemission peaks of the Al 2p and Pt 4f orbitals, which are commonly used in Al and Pt analysis, have a significant overlap. Therefore, the Al 2s peak with a binding energy at 118 eV and the Pt 4d peak with binding energies at 315 and 333 eV were used for the XPS analysis. The relative atomic fractions on the surface of the growing film were calculated using the following equations:

$$\text{Relative A1 2s XPS at\%} = \left(\frac{I_{Al}}{s_{Al}}\right) \Big/ \left(\frac{I_{Al}}{s_{Al}} + \frac{I_{Pt}}{s_{Pt}}\right) \quad (1)$$

$$\text{Relative Pt 4d XPS at \%} = \left(\frac{I_{Pt}}{S_{Pt}}\right) \Big/ \left(\frac{I_{Al}}{S_{Al}} + \frac{I_{Pt}}{S_{Pt}}\right) \quad (2)$$

I_{Al} and I_{Pt} are the measured peak intensities for the Al 2s and Pt 4d XPS peaks. $S_{Al} = 0.753$ and $= 19.1$ are the sensitivity factors for the Al 2s and Pt 4d XPS peaks from the CASA XPS software. The plot of the relative XPS atomic fractions of Al and Pt versus the number of ALD cycles is shown in Fig. 4.

The relative Al and Pt atomic fractions on the surface indicate Pt ALD film growth which qualitatively agrees with the Pt ALD film growth revealed by the XRR analysis. Very little Pt is deposited during the first 25–38 ALD cycles. A rapid increase in the relative Pt atomic fraction is observed at 38–50 ALD cycles. Subsequently, the relative Pt atomic fraction dominates the near surface region composition at >60 cycles. The evolution of the relative atomic fraction with increasing ALD cycles suggests the slow growth of Pt ALD nanoclusters during the first 25–38 cycles. XPS analysis further indicates that the Pt islands may coalesce between 25–38 ALD cycles and then lead to approximately constant Pt ALD after 50 ALD cycles. The dashed lines in Fig. 4 show the fit assuming an exponential decay predicted by the layer-by-layer growth of Pt on the Al_2O_3 substrate.[30] The layer-by-layer growth model is in excellent agreement with the results for >40 ALD cycles.

The thicknesses of the Pt films grown with 0–100 ALD cycles were estimated from the XPS signals using the Thickogram model,[29]

$$\frac{(I_{Al}/s_{Al})}{(I_{Pt}/s_{Pt})} = \frac{\exp(-t/\lambda_{Al}\cos\theta)}{1-\exp(-t/\lambda_{pt}\cos\theta)} \quad (3)$$

The Thickogram model assumes a Pt film with a density of 100% of bulk Pt that has atomically smooth Pt-Al_2O_3 and Pt-vacuum interfaces. Effective attenuation lengths of 1.35 nm for Al 2s and 1.23 nm for Pt 4d photoelectrons in Pt were obtained from the NIST electron effective attenuation length database.[31] The thicknesses of the Pt ALD films grown using 0–100 cycles are shown in Fig. 5.

The Pt film thicknesses obtained from the XRR measurements and adjusted for the density are also shown for comparison in Fig. 5. This density adjusted film thickness is a more accurate measure of the total Pt deposited on the surface and better suited for comparison with the Thickogram calculations. No Al XPS signals were observed for the Pt ALD films grown using 125, 150, 200, and 300 cycles. This behavior indicates that the Al 2s photoelectrons emitted from the underlying Al_2O_3 substrate are completely attenuated by Pt ALD films with thicknesses $\geq$ 4 nm.

Downloaded 27 Apr 2011 to 131.155.110.244. Redistribution subject to AIP license or copyright; see http://jap.aip.org/about/rights_and_permissions

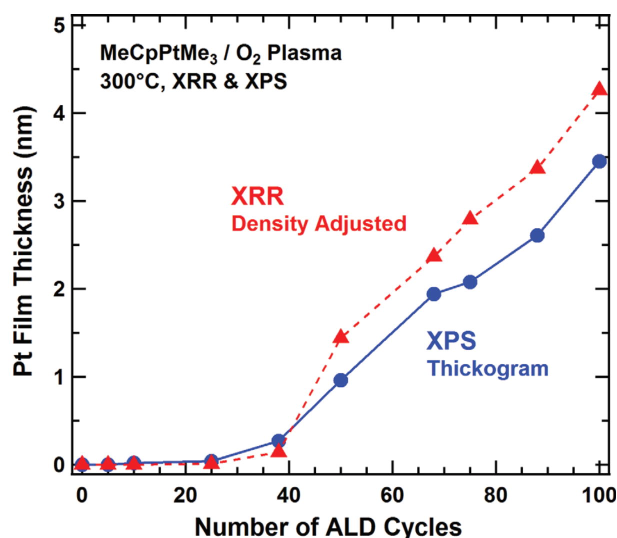

FIG. 5. (Color online) Pt film thicknesses determined using the density-adjusted XRR thickness and the XPS Thickogram model vs number of ALD cycles for Pt ALD films grown on Al_2O_3 using $MeCpPtMe_3$ and O_2 plasma at 300 °C.

The XRR film thicknesses adjusted for film density and the film thicknesses determined by XPS using the Thickogram model are in good agreement. Both sets of film thicknesses show that 25–38 ALD cycles are required to nucleate the Pt ALD film. Some of the discrepancy between the thicknesses determined by the XRR and XPS measurements may be caused by the assumptions in the Thickogram model or a systematic error introduced by uncertainty in the effective attenuation lengths. In addition, the possible presence of pinholes would lead to areas where the Al_2O_3 ALD substrate is exposed or where the localized Pt ALD film thickness is lower than the average film thickness. These areas would lead to proportionally lower attenuation of the Al photoelectrons. Higher emission of Al photoelectrons from these areas would lead to an underestimation of the Pt thickness by XPS analysis.

Depth profile XPS analysis was performed on the Pt ALD film grown using 300 ALD cycles. This Pt ALD film had a thickness of ~15 nm. Appreciable quantities of carbon and oxygen were observed on the surface of the Pt ALD film prior to Ar ion sputtering. These signals most likely originate from adventitious carbon and adsorbed CO, O_2, and H_2O. After sputtering an estimated depth of 1–2 nm, no aluminum, oxygen, carbon, or other impurities were observed in the XPS spectra. Therefore, given the XPS sensitivity, the level of any impurity present in the bulk of the Pt ALD film is $< 1\%$. This conclusion assumes that the Ar^+ sputtering beam does not reduce any PtO_x species or selectively sputter oxygen. The absence of contaminants indicates that the plasma Pt ALD process using $MeCpPtMe_3$ and O_2 plasma produces high purity Pt metal films.

D. Scanning Electron Microscopy

Figure 6(a) presents the SEM image of the initial Al_2O_3 substrate. Figures 6(b) and 6(c) show the SEM images from the Pt ALD samples after 38 and 50 ALD cycles. Figure 7 displays the SEM images from the Pt ALD samples after 68, 75, and 88 cycles. Figure 8 shows the SEM images from the Pt ALD samples after 100, 125, and 150 cycles. The dimensions indicated in Figs. 6–8 are the density adjusted Pt film thicknesses for each sample as determined by the XRR analysis.

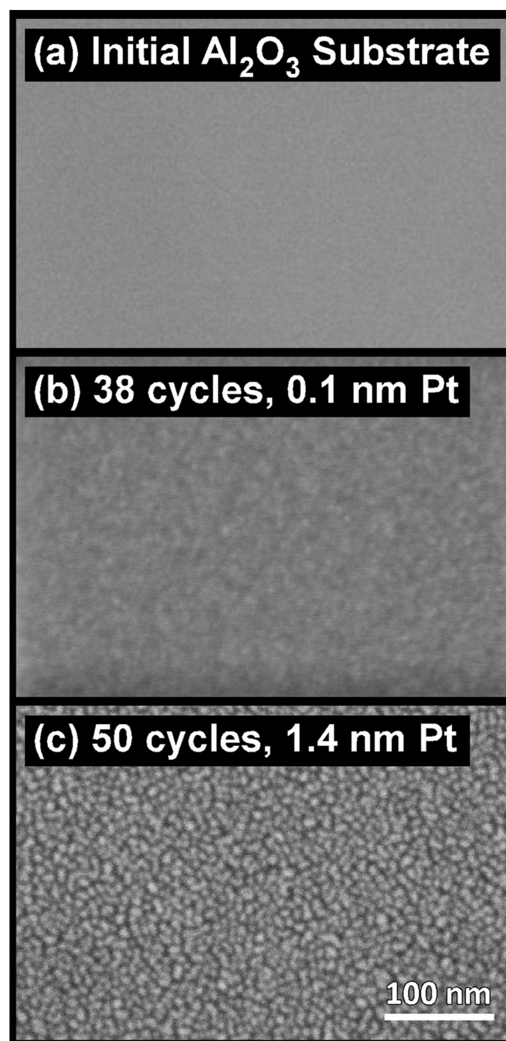

FIG. 6. SEM images of (a) initial Al_2O_3 substrate, (b) after 38 cycles, and (c) after 50 cycles for Pt ALD films grown on Al_2O_3 using $MeCpPtMe_3$ and O_2 plasma at 300 °C. The density-adjusted Pt film thicknesses from XRR analysis are also given.

The SEM images after 38, 50, 68, and 75 ALD cycles suggest that the Pt film nucleates on the Al_2O_3 ALD substrate as discrete nanoclusters. The island diameters are <5 nm after 38 ALD cycles in Fig. 6(b). The Pt nanocluster diameter then increases to ~5 nm after 50 ALD cycles in Fig. 6(c). The islands also become more evenly dispersed and begin to coalesce with adjacent Pt islands. The Pt islands continue to grow laterally and coalesce with neighboring islands after 68 and 75 ALD cycles as shown in Figs. 7(a) and 7(b), respectively. These coalesced islands form corrugated and wormlike structures with typical spacing between adjacent features of ~5–10 nm.

The Pt film density approaches the bulk Pt density as the corrugated Pt structures coalesce into a conformal film. After 88 ALD cycles the corrugated structure is less pronounced in

Downloaded 27 Apr 2011 to 131.155.110.244. Redistribution subject to AIP license or copyright; see http://jap.aip.org/about/rights_and_permissions

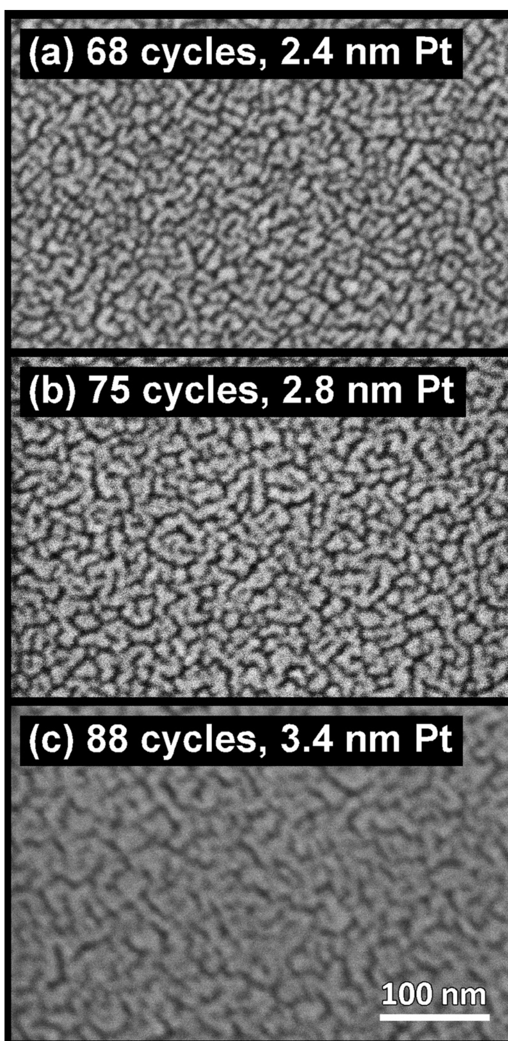

FIG. 7. SEM images after (a) 68 cycles, (b) 75 cycles, and (c) 88 cycles for Pt ALD films grown on Al_2O_3 using $MeCpPtMe_3$ and O_2 plasma at 300 °C. The density-adjusted Pt film thicknesses from XRR analysis are also given.

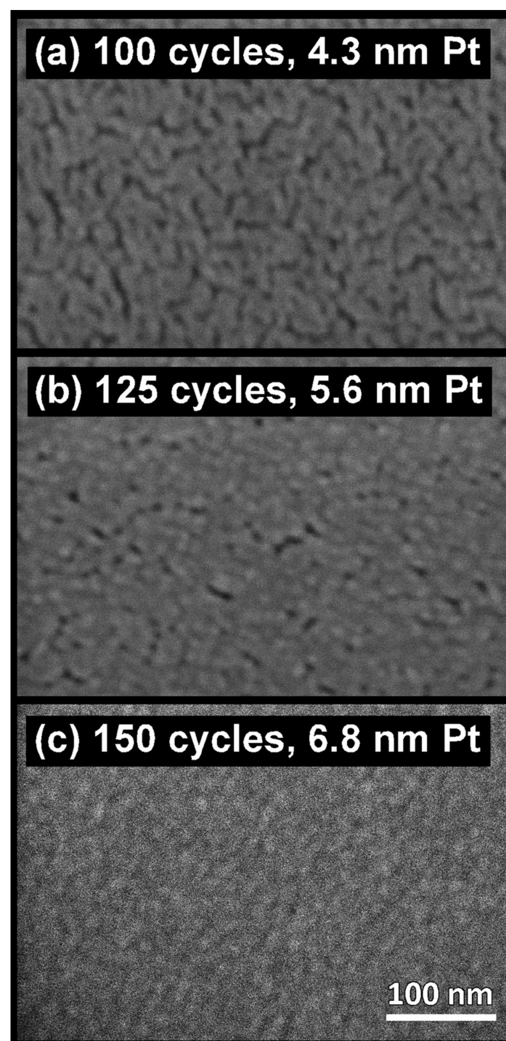

FIG. 8. SEM images after (a) 100 cycles, (b) 125 cycles, and (c) 150 cycles for Pt ALD films grown on Al_2O_3 using $MeCpPtMe_3$ and O_2 plasma at 300 °C. The density-adjusted Pt film thicknesses from XRR analysis are also given.

Fig. 7(c) and the density of the film is 81% of bulk Pt. The Pt ALD film forms a smoother surface morphology after 100 and 125 cycles as revealed by the SEM images in Figs. 8(a) and 8(b), respectively. The Pt ALD film also has a density of 97% of bulk Pt after 125 cycles.

The morphology of the Pt ALD film continues to evolve and shows the presence of island structures with a typical diameter of ~10 nm and density of 97% of bulk Pt after 300 ALD cycles. However, XRR analysis indicates a roughness of only ~0.7 nm RMS after 300 ALD cycles. The low RMS roughness and high density suggests that the 10 nm features are not spherical Pt islands but relatively flat Pt islands on top of an underlying conformal Pt film.

E. Pt ALD Films Grown Under Different Process Parameters

A second set of Pt ALD films were deposited on Al_2O_3 ALD substrates at the University of Colorado using different O_2 plasma process parameters. These O_2 plasma process parameters were an oxygen pressure of 0.3 Torr, an ICP RF power of 600 W, and a plasma exposure time of 5 s. In addition, the Pt ALD films were grown on Al_2O_3 ALD substrates using $MeCpPtMe_3$ and O_2 plasma at 200 °C. This lower temperature was used because of the temperature limitations of the reactor. Figure 9 shows the relative XPS atomic fractions for Al and Pt derived from the Al 2s and Pt 4d XPS signals versus the number of ALD cycles. The Pt ALD nucleation is faster for these O_2 plasma process parameters than the nucleation rate observed in Fig. 4.

XRR scans of the films deposited using 25, 50, 100, and 200 cycles are shown in Fig. 10. A summary of the various film thicknesses grown on Al_2O_3 versus different numbers of ALD cycles using $MeCpPtMe_3$ and O_2 plasma at 200 °C are shown in Table II. The density % is also given in Table II. The films grown using <125 ALD cycles could not be fit using a single Pt film. Reasonable fits could be obtained using a much lower density film or a two-layer film containing a low density film on top of the Pt. For these fits, the low density film was assumed to be PtO_2 with a density of $\rho = 10.2$ g/cm^3. Pt has a density of $\rho = 21.45$ g/cm^3. Note that the densities of these two-layer films were substantially lower than the bulk densities of PtO_2 and Pt. Films that could

Downloaded 27 Apr 2011 to 131.155.110.244. Redistribution subject to AIP license or copyright; see http://jap.aip.org/about/rights_and_permissions

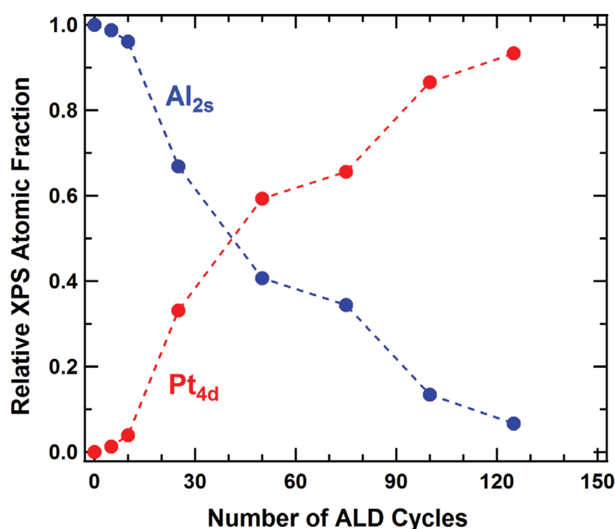

FIG. 9. (Color online) Relative XPS atomic fraction of Al and Pt vs number of ALD cycles for Pt ALD films grown on Al_2O_3 using $MeCpPtMe_3$ and O_2 plasma at 200 °C.

be fit using a single Pt film with the bulk Pt density were not obtained until 125 ALD cycles when the Pt films had a thickness of ∼4 nm.

IV. ADDITIONAL ISSUES

A. Previous Results for Pt ALD on Various Surfaces

Many studies have explored thermal Pt ALD on various substrates using $MeCpPtMe_3$ and O_2. These investigations have all revealed that Pt ALD does not lead to the growth of a continuous and conformal Pt ALD film as expected for ideal ALD. The original Pt ALD films grown using $MeCpPtMe_3$ and O_2 were uniform but they were rough.[12] The Pt ALD films with a thickness of 110 nm displayed a surface roughness of 17 ± 1 nm.[12] This roughness was attributed to the film crystallinity and could also have been affected by difficulties nucleating the initial Pt ALD film.

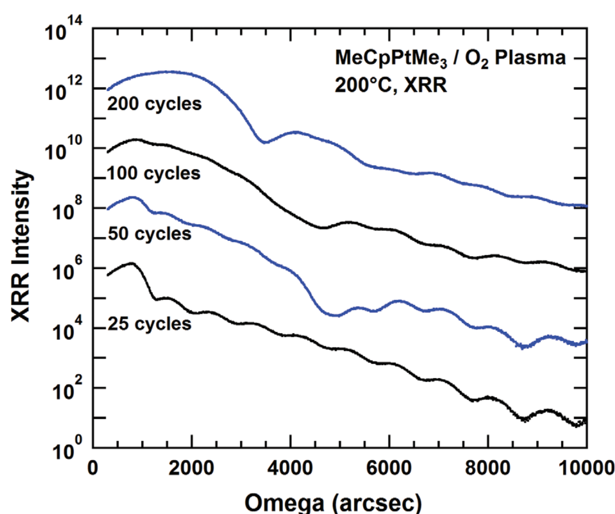

FIG. 10. (Color online) XRR scans for Pt ALD films grown using 25, 50, 100, and 200 ALD cycles on Al_2O_3 using $MeCpPtMe_3$ and O_2 plasma at 200 °C. Summary of the data from XRR scans for the various Pt ALD films grown using different numbers of ALD cycles is given in Table II.

TABLE II. Summary of the XRR thickness and XRR density % of bulk Pt for films grown on Al_2O_3 vs number of ALD cycles using $MeCpPtMe_3$ and O_2 plasma under different process conditions at 200 °C.

Cycles	XRR Thickness (nm)	XRR Density %
25	1.78 (PtO_2)	76 (PtO_2)
50	1.38 (PtO_2)	77 (PtO_2)
	1.99 (Pt)	62 (Pt)
75	1.24 (PtO_2)	70 (PtO_2)
	3.77 (Pt)	64 (Pt)
100	1.59 (PtO_2)	78 (PtO_2)
	2.59 (Pt)	80 (Pt)
125	3.99 (Pt)	97 (Pt)
150	4.89 (Pt)	92 (Pt)
200	5.79 (Pt)	99 (Pt)

Thermal Pt ALD was also performed using $MeCpPtMe_3$ and O_2 on yttria-stabilized zirconia and oxide-covered silicon.[15] These studies revealed that Pt ALD films thinner than 18.3 nm were discontinuous and porous.[15] This porosity was attributed to an island growth mechanism in which islands of fixed lateral dimension first grow to a given height before spreading to cover the entire surface. Additional studies by the same group also observed that 72 cycles of thermal Pt ALD on various sputtered metals resulted in Pt clusters.[21] Various degrees of Pt coverage on the different metals were observed that correlated with expectations from relative surface energies.[21]

Platinum nanoclusters were also observed for thermal Pt ALD using $MeCpPtMe_3$ and O_2 on $SrTiO_3$(001) and strontium titinate nanocubes.[13,14] Atomic force microscope and SEM images both revealed a fine granular structure composed of Pt nanoparticles that nucleated and then coalesced with increasing ALD cycles. The nucleation of the Pt nanoclusters was more rapid on $SrTiO_3$ than other oxide substrates. The growing Pt islands grew together and produced a continuous film after 40 ALD cycles at an approximate thickness of ∼8 nm.[13] Additional studies by the same group also revealed that thermal Pt ALD forms Pt nanoparticles on high surface area Al_2O_3, TiO_2 and $SrTiO_3$ supports.[20] TEM images revealed the deposition of fairly monodisperse Pt nanoclusters that may have catalytic applications.

Additional studies on other substrates also indicate that thermal Pt ALD using $MeCpPtMe_3$ and O_2 does not produce continuous and conformal Pt films. Pt nanoparticles were observed on carbon aerogels that exhibited high catalytic activity for CO oxidation.[16] Thermal Pt ALD on carbon nanotubes also produced Pt nanoparticles that may have applications for proton-exchange membrane fuel cells.[18] Thermal Pt ALD performed in a fluidized bed reactor on micron-sized mesoporous silica gel also revealed Pt nanoparticles.[17]

The previous studies of thermal Pt ALD are all consistent with nucleation difficulties using the $MeCpPtMe_3$ and O_2 reactants on a variety of substrates. Pt nanoclusters are obtained instead of a smooth conformal Pt film that would be expected for ideal ALD. Continuous Pt films may not be possible using thermal Pt ALD until film thicknesses are >20 nm on all substrates except $SrTiO_3$. In contrast, plasma Pt

Downloaded 27 Apr 2011 to 131.155.110.244. Redistribution subject to AIP license or copyright; see http://jap.aip.org/about/rights_and_permissions

ALD is capable of much more rapid nucleation and growth.[22] This study has shown that plasma Pt ALD with O_2 plasma can lead to nearly continuous and conformal Pt films on Al_2O_3 at thicknesses of ~4–5 nm.

B. Mechanism of Pt ALD Nucleation and Growth on Al_2O_3 Substrates

The mechanism of thermal Pt ALD using $MeCpPtMe_3$ and O_2 has been studied using quartz crystal microbalance and quadrupole mass spectrometry studies.[32] Additional studies of the surface reactions using gas phase infrared spectroscopy[23] and theoretical studies of the reaction mechanism[33] are consistent with partial oxidative dehydrogenation and hydrogenation of the methylcyclopentadienyl and methyl ligands during the $MeCpPtMe_3$ exposure. These reactions lead to the evolution of CO_2, CH_4, and some H_2O from the surface.[34] During the oxygen exposure, oxygen gas dissociatively adsorbs on the Pt surface and the remaining organic carbonaceous species are effectively burned off via catalytic oxidation leading to the evolution of CO_2 and H_2O from the surface. The Pt surface also forms a surface oxide phase such as PtO_2 during the oxygen exposure.[35,36]

The surface reactions during plasma Pt ALD involve a more active form of oxygen produced by the O_2 plasma. The surface reactions during plasma Pt ALD are believed to be fairly similar to the surface reactions during thermal Pt ALD. The change would be that molecular oxygen for thermal Pt ALD is replaced by atomic oxygen for plasma Pt ALD. Nucleation is difficult because the initial substrate may not supply oxygen to initiate the reaction. The $MeCpPtMe_3$ may react with hydroxyl groups as suggested by theoretical studies.[33] However, this reaction may not be efficient. The benefit of the O_2 plasma may be to provide extra oxygen atoms to the surface to initiate the reaction by facilitating the reactive adsorption of $MeCpPtMe_3$. In addition, the O_2 plasma may be more effective at promoting the formation of PtO_x phases with higher oxygen content relative to the PtO_x phases formed by O_2 gas exposures.[36]

High exposures of O_2 plasma can oxidize Pt to form PtO_x species such as PtO_2.[22] The low density of the Pt-containing films grown under different plasma process parameters using <125 cycles at 200 °C in Figs. 9 and 10 may be partially explained by the presence of low density PtO_x films. However, XPS analysis was unable to distinguish between PtO_2 and Pt because of the small chemical shift in the Pt 4f peaks for PtO_2 and the inherent difficulty in deconvolving the Pt 4f and Al 2p peaks which overlap significantly. The deposition of PtO_x films is consistent with the observation that PtO_2 ALD films can be grown using $MeCpPtMe_3$ and longer O_2 plasma exposures or lower temperatures.[22] The importance of temperature was also observed in studies of thermal Pt ALD using $Pt(acac)_2$ and ozone.[37] Amorphous PtO_x films were deposited at lower temperatures of 120 and 130 °C and metallic Pt films were grown at ≥140 °C.[37]

The low density Pt film could also be rationalized by a corrugated and wormlike structure similar to the structure observed by the SEM images in Figs. 6–8 for the Pt ALD films grown at 300 °C. However, the Pt ALD films grown at 200 °C have not been examined using SEM. The results in Table II reveal that the low density films grown at 200 °C make a transition to high density pure Pt films after >100 ALD cycles. The critical thickness for this transition is ~4 nm.

The presence of PtO_x nanoclusters may be important in the nucleation period because of the role of oxygen in oxidative dehydrogenation of the ligands of $MeCpPtMe_3$ during the $MeCpPtMe_3$ exposure. Earlier studies have demonstrated that the oxygen affinity of Pt increases significantly below a nanoparticle size of approximately 5–10 nm.[38] PtO_x species are likely formed during the nucleation period when small Pt-containing islands below 5 nm in size are present on the surface. As the PtO_x clusters increase in size, the oxygen affinity of the Pt-containing clusters decreases, and eventually favors the formation of pure Pt islands with PtO_x surface species. The formation of PtO_x clusters during the nucleation phase would enhance the Pt ALD growth rate by providing more adsorbed oxygen to react with $MeCpPtMe_3$ during the $MeCpPtMe_3$ exposures. Recent x-ray absorption near edge structure and extended x-ray absorption fine structure studies confirm the presence of PtO_x on the surface of the initial oxide support during thermal Pt ALD.[20]

C. Prospects for Growth of Ultrathin Conformal Pt ALD Films

The results of this study indicate that an ultrathin continuous Pt ALD film can be deposited on Al_2O_3 ALD substrates using plasma ALD with $MeCpPtMe_3$ and O_2 plasma. Readily available oxygen atoms on the Al_2O_3 substrate from the O_2 plasma facilitate more rapid Pt ALD nucleation compared with thermal Pt ALD. The nucleation of the plasma Pt ALD growth is restricted during the first 25–38 ALD cycles. During this nucleation phase, Pt or PtO_x nanoclusters are probably present on the Al_2O_3 surface. These islands grow and then coalesce. If a high density of nanoclusters can be formed during the initial $MeCpPtMe_3$ and O_2 plasma cycles, then the islands can more readily grow together to form a continuous Pt film. The growth of ultrathin continuous Pt films requires a high density of Pt or PtO_x islands during the nucleation phase.

The ideal substrate for the growth of ultrathin and conformal Pt ALD films would have a surface energy higher than the surface energy of Pt. This definition of an ideal substrate ignores the details of the interface adhesion energies and the surface chemistry and surface kinetics. The simple idea is that a substrate with a surface energy higher than Pt would promote layer-by-layer Pt growth because a continuous Pt coating on the substrate would reduce the system surface energy. Pt has a fairly high surface energy of 2.5 J/m^2.[39] Very few metals have higher surface energies than Pt. One metal that has a higher surface energy is tungsten (W) with a surface energy of 3.3 J/m^2.[39] A Pt film would be predicted to coat W because the surface energy would be reduced from 3.3 J/m^2 to 2.5 J/m^2.

Previous surface science experiments demonstrate that platinum wets tungsten surfaces and grows in a Frank-van der Merwe layer-by-layer growth mode. Auger electron spectroscopy experiments and temperature programmed desorption

Downloaded 27 Apr 2011 to 131.155.110.244. Redistribution subject to AIP license or copyright; see http://jap.aip.org/about/rights_and_permissions

experiments on Pt overlayers on W(110) revealed that Pt grows in the Frank-van der Merwe mode for the first few layers.[40] Additional high-resolution soft-x-ray photoelectron spectroscopy studies revealed that Pt films grow in the layer-by-layer mode on W(111).[41] Low energy electron diffraction and x-ray photoelectron diffraction investigations also reveal that Pt grows pseudomorphically on W(100) for several monolayers before forming distorted hexagonal structures.[42] These studies all argue that Pt films should easily wet tungsten substrates.

Preliminary experiments have been performed for plasma Pt ALD using $MeCpPtMe_3$ and H_2 plasma on W ALD films on Al_2O_3 substrates.[43] These experiments have shown that plasma Pt ALD using $MeCpPtMe_3$ and H_2 plasma can nucleate more rapidly on W ALD films than plasma ALD using $MeCpPtMe_3$ and O_2 plasma on Al_2O_3 ALD substrates. The more rapid nucleation leads to ultrathin and continuous Pt ALD films with thicknesses <2–3 nm. The results of this nucleation and growth study will be presented in a future publication.

V. CONCLUSIONS

The nucleation and growth of Pt ALD on Al_2O_3 substrates was examined using $MeCpPtMe_3$ and O_2 plasma as the reactants. A variety of techniques including SE, XRR, XPS, and SEM were used to study the nucleation of Pt ALD on Al_2O_3 ALD surfaces at 300 °C. These techniques revealed that plasma Pt ALD does not nucleate and grow immediately on the Al_2O_3 ALD substrates. An initial nucleation delay exists before measurable Pt is monitored on the Al_2O_3 surface. However, plasma Pt ALD with $MeCpPtMe_3$ and O_2 plasma nucleates and grows much more rapidly than thermal Pt ALD with $MeCpPtMe_3$ and O_2.

Negligible Pt ALD is measured during the first 25–38 ALD cycles during plasma Pt ALD using O_2 plasma. The Pt ALD growth rate then increases during the next 12 ALD cycles and reaches the steady state linear growth regime at >50 ALD cycles. A steady state Pt ALD growth rate of ~ 0.05 nm/cycle is obtained for >50 ALD cycles. The measurements suggest that the plasma Pt ALD process forms a number of dispersed nanoclusters during the first 38 ALD cycles. These islands may be composed of PtO_x that could supply oxygen to react with $MeCpPtMe_3$ during the $MeCpPtMe_3$ exposure. These islands then merge rapidly during the next 12 cycles and form a Pt-containing film that is corrugated and wormlike with a thickness of ~ 2–3 nm. These Pt-containing films have a density of only 50–70% of bulk Pt.

Films that are much smoother and have densities that are consistent with bulk Pt are observed after >100 ALD cycles. These higher density films are obtained when the Pt ALD film is ≥ 4–5 nm in thickness. Plasma Pt ALD is able to produce much thinner continuous Pt films after fewer ALD cycles than thermal Pt ALD. Plasma Pt ALD must be able to form a much higher density of Pt-containing islands on the initial substrate that quickly merge with other islands to form a thin continuous Pt film. Even thinner Pt ALD films may be possible for plasma Pt ALD on initial substrates with higher surface energies than Pt such as W.

ACKNOWLEDGMENTS

The work at the University of Colorado was supported by General Motors Research and Development. Additional support was provided by the Defense Advanced Research Project Agency (DARPA). Some of the equipment used in this research was provided by the Air Force Office of Scientific Research. L.B and S.M.G. thank Advanced Energy in Ft. Collins, CO, for the plasma source used for the plasma Pt ALD at the University of Colorado. The authors acknowledge H.C.M. Knoops of the Eindhoven University of Technology for his contribution to the depositions. The work at the Eindhoven University of Technology was financially supported by the Dutch Technology Foundation STW.

[1]S. M. George, Chem. Rev. **110**, 111 (2010).
[2]T. Suntola, Thin Solid Films **216**, 84 (1992).
[3]C. T. Campbell, Surf. Sci. Rep. **27**, 1 (1997).
[4]D. N. Goldstein and S. M. George, Appl. Phys. Lett. **95**, 143106 (2009).
[5]D. N. Goldstein and S. M. George, "Surface poisoning in the nucleation and growth of palladium atomic layer deposition with $Pd(hfac)_2$ and formalin," Thin Solid Films (in press).
[6]F. H. Fabreguette, R. A. Wind, and S. M. George, Appl. Phys. Lett. **88**, 013116 (2006).
[7]Z. A. Sechrist, F. H. Fabreguette, O. Heintz, T. M. Phung, D. C. Johnson, and S. M. George, Chem. Mater. **17**, 3475 (2005).
[8]R. W. Wind, F. H. Fabreguette, Z. A. Sechrist, and S. M. George, J. Appl. Phys. **105**, 074309 (2009).
[9]H. A. Gasteiger, S. S. Kocha, B. Sompalli, and F. T. Wagner, Appl. Catal., B **56**, 9 (2005).
[10]V. Mehta and J. S. Cooper, J. Power Sources **114**, 32 (2003).
[11]F. T. Wagner, B. Lakshmanan, and M. F. Mathias, J. Phys. Chem. Lett. **1**, 2204 (2010).
[12]T. Aaltonen, M. Ritala, T. Sajavaara, J. Keinonen, and M. Leskela, Chem. Mater. **15**, 1924 (2003).
[13]S. T. Christensen, J. W. Elam, B. Lee, Z. Feng, M. J. Bedzyk, and M. C. Hersam, Chem. Mater. **21**, 516 (2009).
[14]S. T. Christensen, J. W. Elam, F. A. Rabuffetti, Q. Ma, S. J. Weigand, B. Lee, S. Seifert, P. C. Stair, K. R. Poeppelmeier, M. C. Hersam, and M. J. Bedzyk, Small **5**, 750 (2009).
[15]X. Jiang and S. F. Bent, J. Electrochem. Soc. **154**, D648 (2007).
[16]J. S. King, A. Wittstock, J. Biener, S. O. Kucheyev, Y. M. Wang, T. F. Baumann, S. K. Giri, A. V. Hamza, M. Baeumer, and S. F. Bent, Nano Lett. **8**, 2405 (2008).
[17]J. H. Li, X. H. Liang, D. M. King, Y. B. Jiang, and A. W. Weimer, Appl. Catal., B **97**, 220 (2010).
[18]C. Liu, C. C. Wang, C. C. Kei, Y. C. Hsueh, and T. P. Perng, Small **5**, 1535 (2009).
[19]A. J. M. Mackus, J. J. L. Mulders, M. C. M. van de Sanden, and W. M. M. Kessels, J. Appl. Phys. **107**, 116102 (2010).
[20]W. Setthapun, W. D. Williams, S. M. Kim, H. Feng, J. W. Elam, F. A. Rabuffetti, K. R. Poeppelmeier, P. C. Stair, E. A. Stach, F. H. Ribeiro, J. T. Miller, and C. L. Marshall, J. Phys. Chem. C **114**, 9758 (2010).
[21]J. H. Shim, X. Jiang, S. F. Bent, and F. B. Prinz, J. Electrochem. Soc. **157**, B793 (2010).
[22]H. C. M. Knoops, A. J. M. Mackus, M. E. Donders, M. C. M. van de Sanden, P. H. L. Notten, and W. M. M. Kessels, Electrochem. Solid State Lett. **12**, G34 (2009).
[23]W. M. M. Kessels, H. C. M. Knoops, S. A. F. Dielissen, A. J. M. Mackus, and M. C. M. van de Sanden, Appl. Phys. Lett. **95**, 013114 (2009).
[24]J. L. van Hemmen, S. B. S. Heil, J. H. Klootwijk, F. Roozeboom, C. J. Hodson, M. C. M. van de Sanden, and W. M. M. Kessels, J. Electrochem. Soc. **154**, G165 (2007).
[25]E. Langereis, H. C. M. Knoops, A. J. M. Mackus, F. Roozeboom, M. C. M. van de Sanden, and W. M. M. Kessels, J. Appl. Phys. **102**, 083517 (2007).
[26]S. B. S. Heil, J. L. van Hemmen, C. J. Hodson, N. Singh, J. H. Klootwijk, F. Roozeboom, M. de Sanden, and W. M. M. Kessels, J. Vac. Sci. Technol. A **25**, 1357 (2007).
[27]E. Langereis, S. B. S. Heil, H. C. M. Knoops, W. Keuning, M. C. M. van de Sanden, and W. M. M. Kessels, J. Phys. D:Appl. Phys. **42**, 073001 (2009).

Downloaded 27 Apr 2011 to 131.155.110.244. Redistribution subject to AIP license or copyright; see http://jap.aip.org/about/rights_and_permissions

[28]E. Chason and T. M. Mayer, Crit. Rev. Solid State Mater. Sci. **22**, 1 (1997).
[29]P. J. Cumpson, Surf. Interface Anal. **29**, 403 (2000).
[30]R. W. Paynter, J. Electron Spectrosc. **169**, 1 (2009).
[31]C. J. Powell and A. Jablonski, *Electron Effective Attenuation Length Database* (National Institute of Standards and Technology, Gaithersburg, 2003).
[32]T. Aaltonen, A. Rahtu, M. Ritala, and M. Leskela, Electrochem, Solid State Lett. **6**, C130 (2003).
[33]S. D. Elliott, Langmuir **26**, 9179 (2010).
[34]Z. Ma and F. Zaera, Surf. Sci. Rep. **61**, 229 (2006).
[35]C. Ellinger, A. Stierle, I. K. Robinson, A. Nefedov, and H. Dosch, J. Phys.:Condens. Matter **20**, 184013 (2008).
[36]J. F. Weaver, H. H. Kan, and R. B. Shumbera, J. Phys.:Condens. Matter **20**, 184015 (2008).
[37]J. Hamalainen, F. Munnik, M. Ritala, and M. Leskela, Chem. Mater. **20**, 6840 (2008).
[38]K. J. J. Mayrhofer, B. B. Blizanac, M. Arenz, V. R. Stamenkovic, P. N. Ross, and N. M. Markovic, J. Phys. Chem. B **109**, 14433 (2005).
[39]L. Vitos, A. V. Ruban, H. L. Skriver, and J. Kollar, Surf. Sci. **411**, 186 (1998).
[40]S. M. Shivaprasad, R. A. Demmin, and T. E. Madey, Thin Solid Films **163**, 393 (1988).
[41]J. J. Kolodziej, T. E. Madey, J. W. Keister, and J. E. Rowe, Phys. Rev. B **65**, 075413 (2002).
[42]R. W. Judd, M. A. Reichelt, E. G. Scott, and R. M. Lambert, Surf. Sci. **185**, 529 (1987).
[43]L. Baker, A. S. Cavanagh, D. Seghete, S. M. George, A. J. M. Mackus, W. M. M. Kessels, Z. Y. Liu and F. T. Wagner, Presentations at Telluride Summer Research Conference on Semiconductor Surface Chemistry, Telluride, Colorado, July 26, 2010; Baltic Atomic Layer Deposition (BALD2010) and Germany Atomic Layer Deposition (GerALD2), Hamburg, Germany, September 16, 2010; and AVS 57th International Symposium, Albuquerque, New Mexico, October 19, 2010.

Downloaded 27 Apr 2011 to 131.155.110.244. Redistribution subject to AIP license or copyright; see http://jap.aip.org/about/rights_and_permissions